TUDelft

Delft University of Technology

Experimental and Theoretical Studies of the Site Occupancy and Luminescence of Ce^{3+} in LiSr$_4$(BO$_3$)$_3$ for Potential X-ray Detecting Applications

Yang, Yunlin; Lou, Bibo; Ou, Yiyi; Su, Fang; Ma, Chong Geng; Duan, Chang Kui; Dorenbos, Pieter; Liang, Hongbin

Important note
To cite this publication, please use the final published version (if applicable).
Please check the document version above.

Experimental and Theoretical Studies on Site Occupancy and Luminescence of Ce^{3+} in LiSr$_4$(BO$_3$)$_3$ for Potential X-ray Detecting Applications

Yunlin Yang[a], Bibo Lou[b], Yiyi Ou[a], Fang Su[a], Chong-Geng Ma[c], Chang-Kui Duan[b], Pieter Dorenbos[d], Hongbin Liang[a],*

[a] MOE Key Laboratory of Bioinorganic and Synthetic Chemistry, KLGHEI of Environment and Energy Chemistry, School of Chemistry, Sun Yat-sen University, Guangzhou 510006, China

[b] CAS Key Laboratory of Microscale Magnetic Resonance and School of Physical Sciences, University of Science and Technology of China, Hefei 230026, China

[c] School of Optoelectronic Engineering & CQUPT-BUL Innovation Institute, Chongqing University of Posts and Telecommunications, Chongqing 400065, China

[d] Faculty of Applied Sciences, Delft University of Technology, 2629 JB, Delft, The Netherlands

Email: cesbin@mail.sysu.edu.cn

ABSTRACT: The Ce^{3+}-doped LiSr$_4$(BO$_3$)$_3$ phosphors have been prepared by a high-temperature solid-state reaction method and the structure refinement of the host compound is performed. The

excitation and emission spectra in vacuum ultraviolet - ultraviolet - visible (VUV-UV-vis) range at cryogenic temperatures reveal that Ce^{3+} ions preferentially occupy eight-coordinated Sr^{2+} sites in $LiSr_4(BO_3)_3$. Such experimental attribution is well corroborated by the calculated 4f-5d transition energies and defect formation energies of Ce^{3+} ions at two distinct Sr^{2+} sites in the first-principles framework. In addition, the doping concentration- and the temperature- dependent luminescence are systematically investigated by luminescence intensity and lifetime measurements, respectively. It shows that the concentration quenching does not occur in the investigated doping range, but the inhomogeneous broadening exists in the concentrated samples. With the estimated thermal quenching activation energy, the discussions on the thermal quenching mechanisms suggest that thermal-ionization process of 5d electron is a dominant channel for thermal quenching of Ce^{3+} luminescence, despite the thermally activated concentration quenching cannot be excluded for the highly doped samples. Finally, the X-ray excited luminescence (XEL) measurement demonstrates the promising applications of the phosphors in X-ray detection.

1. INTRODUCTION

The investigation on luminescence of Ce^{3+} in various host compounds has always been a fascinating field for its fundamental significance and wide applications.[1,2] From the viewpoint of basic research, Ce^{3+} ion shows typical 4f-5d transitions. Due to the simplest $4f^1$ and $5d^1$ electronic configurations of a Ce^{3+} ion in ground and excited states, the energies of f-d transitions of Ce^{3+} in a host compound can provide key reference to those of such lanthanide ions as Eu^{2+} and Pr^{3+} in the same lattice sites of same host compounds.[3] In addition, luminescence of Ce^{3+} is also important for actual applications, and Ce^{3+}-doped materials have been utilized in different fields after years of continuous efforts. For example, $Y_3Al_5O_{12}:Ce^{3+}$ is well-known as a yellow-emitting phosphor

in phosphor-converted light-emitting diodes (pc-LEDs). The scintillators $Lu_2SiO_5:Ce^{3+}$, $LuAlO_3:Ce^{3+}$ and $LnX_3:Ce^{3+}$ (Ln = La, X = Cl/Br; Ln = Lu, X = I) have gained commercial utilizations for detecting of ionizing radiation.[1,4]

Because the crystal field strength has a large influence on the outer 5d orbital of Ce^{3+}, the 4f-5d transition energies of Ce^{3+} may present remarkable variations at different coordination surroundings. Such structural factor, which is controlled by site occupancy, directly governs the various aspects of the luminescence properties.[5-7] Apparently, a clear understanding of the site occupancy of Ce^{3+} in the host compound is crucial for the development of novel lanthanide ions doped luminescent materials with f-d transitions. To our knowledge, a systematic analysis on the crystal field splitting (CFS) and centroid of Ce^{3+} 5d energy levels is a good approach to get insight into the site occupancies of the doping Ce^{3+} ions experimentally.[8,9] Furthermore, the first-principles calculations on the energies of f-d transitions corroborate the site occupancies, and those on the formation and transition energies of Ce^{3+} ions in different sites give the explanations on the preferential occupancies theoretically.[10,11]

$LiSr_4(BO_3)_3$ is an efficient host compound for luminescence of lanthanide ions, which has two Sr^{2+} sites in six-fold coordinated and eight-fold coordinated, respectively.[12] In this paper, the vacuum ultraviolet - ultraviolet - visible (VUV-UV-vis) spectra of Ce^{3+}-doped $LiSr_4(BO_3)_3$ are firstly investigated at cryogenic temperatures in detail to understand the band gap of the host compound, the site occupancy and the 4f-5d transition energies of Ce^{3+} in this site experimentally. Then the first-principles calculations on the f-d transition energies and the formation and transition energies of Ce^{3+} ions in different sites confirm and explain the preferential site occupations theoretically. Besides, the concentration- and the temperature- dependent luminescence characteristics are discussed in terms of the luminescence intensity and lifetime, respectively. And

the possible application of the phosphor for X-ray detection is demonstrated. The work provides a systematic method to understand the preferential site occupancies through the combination of experiments and theoretical calculations. It is conducive to the design of novel luminescent materials.

2. METHODOLOGY

2.1. Experimental Details.

A series of $Li_{1+x}Sr_{4-2x}Ce_x(BO_3)_3$ (x = 0, 0.001, 0.005, 0.01, 0.03) samples were prepared by a traditional high-temperature solid-state reaction method using Li_2CO_3 (analytical reagent, A.R.), $SrCO_3$ (A.R.), CeO_2 (99.99%) and H_3BO_3 (A.R.) as raw materials. After stoichiometrically weighed, thoroughly mixed and ground, all reactants were transferred to the crucibles and sintered in a muffle furnace at 850 °C for 8 hours in a N_2-H_2 reducing gas ambience. When the product returned to room temperature (RT) naturally, it was ground for subsequent characterizations.

The phase purity and the crystal structure of typical samples were characterized by powder X-ray diffraction (XRD) measurements on a Bruker D8 ADVANCE with Cu Kα radiation (λ = 1.5418 Å) at 35 kV and 35 mA. The data were collected over a 2θ range from 10° to 80° with a scanning speed of 10 °/min. The high-quality XRD data for structure Rietveld refinements were recorded over a 2θ range from 10° to 100° with an interval of 0.02°, and the refinements were performed by using TOPAS Academic software.[13] The VUV-UV-vis excitation and emission spectra were measured on the beam line 4B8 of the Beijing Synchrotron Radiation Facility (BSRF, China) under normal operating conditions by using the spectrum of sodium salicylate (o-$C_6H_4OHCOONa$) as a reference. The UV-vis emission and excitation spectra as well as the luminescence decay curves were recorded on an Edinburgh FLS1000 spectrometer. A 450W Xe

lamp was used as the excitation source for steady-state spectra, and an LED laser with a pulse width of 736.7 ps and a pulse repetition rate of 2000 KHz was used for luminescence decay measurements. The detector PET 980 was used for accepting the signal. The temperature-variable spectroscopy test was carried out using an Oxford Optistat DN Model cryostat and controlled by a Mercury iTC Model temperature controller. The X-ray excitation luminescence (XEL) measurement was carried on a Philips PW2253/20 X-ray tube at Delft University of Technology, the Netherlands.[14]

2.2. Computational Details.

To better understand the origin of the measured excitation and emission spectra, we performed first-principles calculations on the formation energies and transition energies of Ce^{3+} in two different Sr^{2+} sites in $LiSr_4(BO_3)_3$. One of the Sr^{2+} ion in the $1 \times 1 \times 1$ supercell containing 272 atoms was replaced with Ce^{3+}, and the structural optimization was carried out under the framework of density functional theory (DFT) utilizing Perdew−Burke−Ernzerof exchange-correlation functional.[15] A Hubbard U of 2.5 eV was adopted for the 4f orbitals of Ce ion. To improve the description on band gaps and Ce^{3+} related energy levels, a modified PBE0 with 31% Hartree−Fock exchange determined by the inverse of the calculated value of the optical dielectric constant, $1/\varepsilon_\infty$. By applying the constrained occupancy method, we obtained the equilibrium structure of the lowest excited state of $LiSr_4(BO_3)_3$: Ce^{3+} that one electron on 4f Kohn-Sham (KS) orbital was excited to the lowest 5d KS orbital. The thermodynamic charge transition level $\epsilon(Ce^{3+/4+})$ is defined as the electron Fermi level to equate the formation energies of Ce^{3+} and Ce^{4+} dopants calculated at their corresponding equilibrium supercells. Relative to the valence band maximum (VBM), $\epsilon(Ce^{3+/4+}) = E_{tot}(Ce^{3+}) - E_{tot}(Ce^{4+}) - \epsilon_{VBM}$, where E_{tot} is the total energy of the

relaxed structure of the LiSr$_4$(BO$_3$)$_3$ supercell containing Ce^{3+} or Ce^{4+} and ϵ_{VBM} is the position of valence band maximum obtained by employing modified PBE0 with Hatree-Fock mixing parameter α = 0.31. The 4f-5d excitation energies were obtained from the differences of the generalized KS eigenvalues calculated at the equilibrium geometric structure of Ce^{3+} supercell. More details about the calculation procedures and their justifications have been given in Ref. 16 and is not elaborated here. The relative formation energies of Ce^{3+} between two sites are calculated with 4f-in-core pseudo potentials, and their relative concentration was estimated by $\omega\exp(-\Delta E_f/k_BT)$, where ω, ΔE_f, k_B, T are the ratio of sites to be occupied, difference in formation energy, the Boltzmann constant and the temperature of sample preparation, respectively.

3. RESULTS AND DISCUSSION

3.1. X-Ray Diffraction (XRD), Structure Refinement and Crystal Structure.
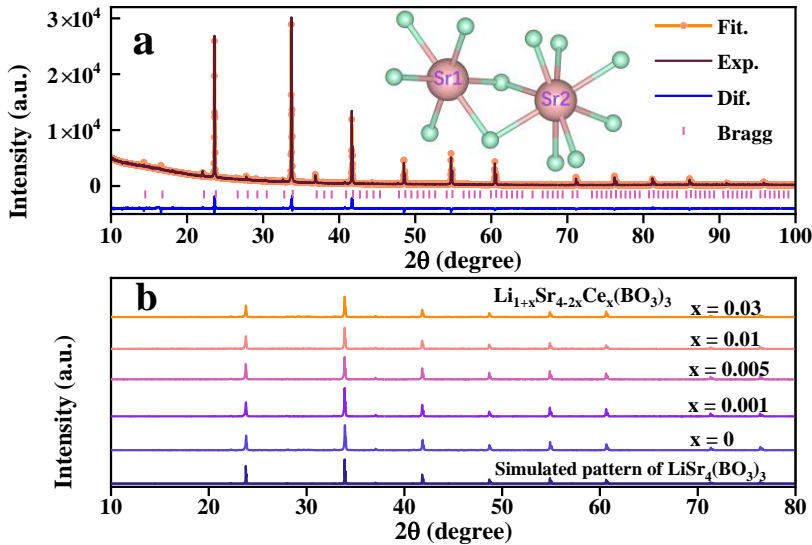
Figure 1. (a) The Rietveld refinement result of XRD data of $LiSr_4(BO_3)_3$ compound at room temperature (RT). The orange-point line means the fitting curve; the black line represents the experimental data; the blue line shows the difference of the experimental data and fitting curve; and the purple bars are the Bragg positions. The inset shows the schematic coordination surroundings of two Sr^{2+} sites in the host lattice. (b) The concentration-dependent XRD patterns of $Li_{1+x}Sr_{4-2x}Ce_x(BO_3)_3$ (x = 0, 0.001, 0.005, 0.01, 0.03); the bottom simulated pattern of $LiSr_4(BO_3)_3$ is done by the VESTA program based on its Crystallographic Information Framework (CIF) file.[17]

To verify the phase purity and check the crystal structure, the high-quality XRD pattern of the host compound $LiSr_4(BO_3)_3$ has been collected and the Rietveld refinement is carried out by using cubic structure as original model as shown in Figure 1a. The values of R_{wp} (~5.98%), R_p (~3.91%) and R_B (~7.87%) all mean a fine fitting result, implying reliable refined indicators for proving impurities free in $LiSr_4(BO_3)_3$. The refined lattice parameters are $a = b = c = 14.949$ Å, $V =$ 3340.484 Å^3 and $Z = 16$. The detailed structural parameters are listed in Table 1. The compound $LiSr_4(BO_3)_3$ crystallizes in cubic structure with space group $Ia\bar{3}d$, in which Sr^{2+} ions occupy two diverse lattice sites.[12] The schematic coordination surroundings of these two Sr^{2+} ions are inserted in the upper right corner of Figure 1a. $Sr^{2+}(1)$ ions are six-fold coordinated to form distorted octahedral $[Sr(1)O_6]$ on the 16a Wyckoff position with S_6 symmetry, while $Sr^{2+}(2)$ ions are eight-coordinated in two-capped trigonal prisms $[Sr(2)O_8]$ on the 48f Wyckoff position with C_2 symmetry. The average Sr-O bond distances for $[Sr(1)O_6]$ and $[Sr(2)O_8]$ polyhedrons are 2.536 Å and 2.630 Å, respectively. The distances of the nearest $Sr^{2+}(1)$-$Sr^{2+}(1)$, $Sr^{2+}(2)$-$Sr^{2+}(2)$ and $Sr^{2+}(1)$-$Sr^{2+}(2)$ are approximately 6.474, 3.665 and 3.738 Å, respectively.

Further, the XRD patterns of Ce^{3+}-doped samples $Li_{1+x}Sr_{4-2x}Ce_x(BO_3)_3$ (x = 0, 0.001, 0.005, 0.01, 0.03) are measured as presented in Figure 1b. Since the standard XRD card of $LiSr_4(BO_3)_3$ is not found in the powder diffraction files (PDF) database, the simulated pattern of $LiSr_4(BO_3)_3$ at the bottom of the graph is obtained using VESTA program according to its CIF file.[17] For the samples with different doping contents, their XRD patterns are identical to the simulated one, and all diffraction peaks can be indexed to the simulated pattern, indicating that these Ce^{3+}-doped samples are without impurities and this can be further confirmed by the luminescence spectra in Section 3.2. In addition, the observations imply that the doping Ce^{3+} ions do not clearly affect the crystal structure of $LiSr_4(BO_3)_3$ host. Considering the similar ionic radii of Ce^{3+} and Sr^{2+} ($r(Ce^{3+})$ = 1.01 Å, $r(Sr^{2+})$ = 1.18 Å, for C.N. (coordination number) = 6; $r(Ce^{3+})$ = 1.14 Å, $r(Sr^{2+})$ = 1.26 Å, for C.N. = 8)[18], Ce^{3+} ions are assumed to enter Sr^{2+} sites. In Sections 3.2-3.3, we will discuss the site occupancy through experimental luminescence spectra and theoretical calculations in detail.

Table 1. The refined structural parameters of $LiSr_4(BO_3)_3$ at RT

Atom	Wyckoff position	x	y	z	Occ.	Beq.
Sr1	16a	0	0	0	1	1.48
Sr2	48f	0	0.25	-0.001	1	0.84
Li	16b	0.125	0.125	0.125	1	1.60
B	96h	0.163	0.352	0.125	1	0.24
O1	96h	-0.020	0.272	0.041	1	0.55
O2	96h	0.264	0.365	0.125	1	1.89

3.2. Excitation/Emission Wavelength Dependencies of Luminescence of $Li_{1.001}Sr_{3.998}Ce_{0.001}(BO_3)_3$.

Figure 2. (a) The highest height-normalized excitation (λ_{em} = 390, 400, 418, 420, 450, 470 and 485 nm) and emission (λ_{ex} = 268, 286 and 332 nm) spectra of the sample $Li_{1.001}Sr_{3.998}Ce_{0.001}(BO_3)_3$ at RT. (b) The luminescence decay curves (λ_{ex} = 320 nm, λ_{em} = 402, 420, 450 and 473 nm) of the sample $Li_{1.001}Sr_{3.998}Ce_{0.001}(BO_3)_3$ at 78 K.
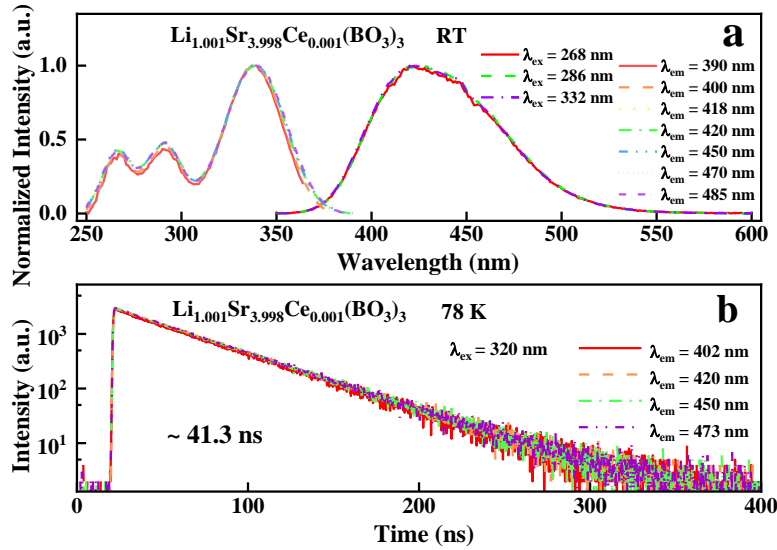
Figure 2a displays the highest height-normalized excitation (λ_{em} = 390, 400, 418, 420, 450, 470 and 485 nm) and emission (λ_{ex} = 268, 286 and 332 nm) spectra of the sample $Li_{1.001}Sr_{3.998}Ce_{0.001}(BO_3)_3$ at RT for comparison. Herein, the wavelengths 268, 286 and 332 nm are close to the peaks of three bands in the excitation spectra, and the wavelengths 390, 400, 418, 420, 450, 470 and 485 nm are near 35%, 65%, 100%, 100%, 80%, 55% and 30% of the emission peak, respectively. Under varied wavelengths excitation, three emission curves almost overlap with one another. Meantime, seven normalized excitation spectra also nearly overlap by monitoring the selected emission wavelengths. The observations suggest that the sample does not contain any

impurity which affects the luminescence in this spectral range, and Ce^{3+} ions occupy only one kind of sites in this sample.

Upon 320 nm excitation, the luminescence decay curves of $Li_{1.001}Sr_{3.998}Ce_{0.001}(BO_3)_3$ of different wavelengths emission are recorded in Figure 2b. All curves overlap and the luminescence lifetime of $Li_{1.001}Sr_{3.998}Ce_{0.001}(BO_3)_3$ is exponentially-fitted to be approximately ~41.3 ns at 78 K. The observation further illustrates the existence of only a single kind of Ce^{3+} luminescence center in the host compound and the inhomogeneous broadening effect is not pronounced in this diluted sample $Li_{1.001}Sr_{3.998}Ce_{0.001}(BO_3)_3$.[19]

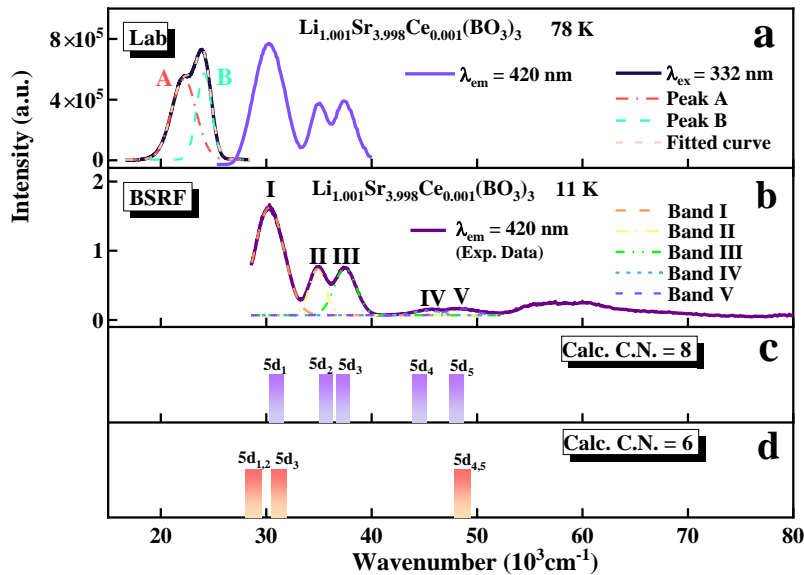## 3.3. VUV-UV-vis Luminescence of $Li_{1.001}Sr_{3.998}Ce_{0.001}(BO_3)_3$ at Cryogenic Temperatures and Site Occupancy of Ce^{3+}.

Figure 3. (a) The lab UV excitation (λ_{em} = 420 nm) and UV-vis emission (λ_{ex} = 332 nm) spectra of the sample $Li_{1.001}Sr_{3.998}Ce_{0.001}(BO_3)_3$ at 78 K. (b) The synchrotron radiation VUV-UV excitation

spectrum (λ_{em} = 420 nm) of $Li_{1.001}Sr_{3.998}Ce_{0.001}(BO_3)_3$ at 11 K. (c, d) The calculated 4f-5d$_j$ (j = 1-5) transition energies of Ce^{3+} ions in two Sr^{2+} sites of $LiSr_4(BO_3)_3$.

To clarify the site occupancy and the 5d energies of Ce^{3+} in this host compound, the VUV-UV-vis luminescence spectra of sample $Li_{1.001}Sr_{3.998}Ce_{0.001}(BO_3)_3$ are collected at cryogenic temperatures. The purple line in Figure 3a presents the UV excitation (λ_{em} = 420 nm) spectrum of this sample using lab Edinburgh FLS1000 spectrometer at 78 K. Three distinct broad bands are seen with maxima at about 30.2×10^3 cm^{-1} (331 nm, 3.74 eV), 35.0×10^3 cm^{-1} (286 nm, 4.33 eV) and 37.4×10^3 cm^{-1} (267 nm, 4.64 eV), respectively. The lowest 4f-5d excitation band of Ce^{3+} in $LiSr_4(BO_3)_3$ has been reported around 340-356 nm range, which are in largely agreement with the value observed in Figure 3a.[20-22] The deviation may be the result of different measurement instruments, temperatures and so on.

The black line in Figure 3a shows the emission spectrum of sample $Li_{1.001}Sr_{3.998}Ce_{0.001}(BO_3)_3$ upon 332 nm excitation at 78 K. The band position is consistent with that in Figure 2a but the spectral resolution is better due to low-temperature condition. It consists of a main band and a shoulder band at shorter wavenumber side. The spectrum can be well-fitted with a sum of two Gaussian functions. Accordingly, two band peaks are estimated at about 22.2×10^3 cm^{-1} (Peak A: 450 nm, 2.75 eV) and 24.1×10^3 cm^{-1} (Peak B: 415 nm, 2.99 eV), respectively. Their energy separation (about 1.90×10^3 cm^{-1}, 0.24 eV) corresponds to typical value of $^2F_{5/2}$ and $^2F_{7/2}$ spin-orbit split 4f ground states of Ce^{3+}. From the energy difference between the band maxima of $^2F_{5/2}$-5d$_1$ transition in excitation (3.74 eV) and emission (2.99 eV) spectra, the Stokes shift of Ce^{3+} in $LiSr_4(BO_3)_3$ is evaluated to be 0.75 eV, indicating that the 5d electrons of Ce^{3+} in $LiSr_4(BO_3)_3$ experience a strong effect of electron-phonon interaction with the coordination environment.[3]

Figure 3b exhibits the synchrotron radiation VUV-UV excitation (λ_{em} = 420 nm) spectrum of $Li_{1.001}Sr_{3.998}Ce_{0.001}(BO_3)_3$ recorded with the beamline 4B8 of the Beijing Synchrotron Radiation Facility (BSRF) at 11 K. The whole excitation profile includes the host-related absorption with energy above about 52.2×10^3 cm^{-1} and the 4f-5d transitions of Ce^{3+} ions below this wavenumber. First, the band gap of the host compound $LiSr_4(BO_3)_3$ is evaluated according to the spectrum in Figure 3b. The host exciton creation energy (E^{ex}) is found at about 56.8×10^3 cm^{-1} (~7.04 eV, 176 nm). This assignment can be further confirmed by the synchrotron radiation VUV-UV excitation spectrum of $Li_{1.001}Sr_{3.998}Gd_{0.001}(BO_3)_3$ sample in Figure S1, in which an evident excitonic absorption band with a maximum at about 175 nm is observed when the 312 nm emission of Gd^{3+} $^6P_{7/2} \rightarrow {^8S_{7/2}}$ transition is monitored. Besides, a conspicuous host-related band has been observed near about 7 eV of the isomorphic compound $NaSr_4(BO_3)_3$.[23] Considering the electron transfer from upper valence band to the conduction band bottom, the optical bandgap value of the host compound should add the electron-hole binding energy of exciton to the host exciton creation absorption energy (E^{ex}). The binding energy can be estimated to be $0.008 \times (E^{ex})^2$.[24] In our case, by adding the electron-hole binding energy to exciton creation energy, the bandgap energy of $LiSr_4(BO_3)_3$ compound between upper valence band and conduction band bottom is calculated to be ~7.44 eV.

Then, we discuss the 4f-5d excitation bands of Ce^{3+} ions in Figure 3b. As mentioned in Section 3.2, Ce^{3+} ions only enter one type of Sr^{2+} sites in $LiSr_4(BO_3)_3$. Hence, at most five 4f-5d transition bands might occur in excitation spectrum. This is exactly what we find in $28.6 \times 10^3 - 52.2 \times 10^3$ cm^{-1} range of the spectrum at 11 K, which contains a strong band (I), two medium bands (II, III) and two very weak overlapping bands. The positions and profiles of three obvious low-energy bands (I-III) are consistent with those in Figure 3a. To better evaluate these excitation peaks, a

sum of five Gaussian functions is adopted to fit the curve at this range. The peak maxima of these bands are estimated to be ~30.2×10^3 cm^{-1} (band I, 3.74 eV, 331 nm), ~34.9×10^3 cm^{-1} (band II, 4.33 eV, 286 nm), ~37.5×10^3 cm^{-1} (band III, 4.64 eV, 267 nm), ~45.2×10^3 cm^{-1} (band IV, 5.61 eV, 221 nm) and ~48.5×10^3 cm^{-1} (band V, 6.01 eV, 206 nm), which are attributed to the Ce^{3+} transitions from the 4f ground state to the first to fifth 5d ($5d_{1-5}$) excitation states, respectively. The different intensity distributions of five excitation bands may relate to the energy separation between the conduction band minimum (CBM) and the $5d_{1-5}$ multiplets as shown in Figure 7 of Section 3.5 (vide infra). The $5d_1$ is fairly below the CBM in energy, so the $4f$-$5d_1$ excitation band is strong; the $5d_{2,3}$ energy levels are close to the CBM, hence the $4f$-$5d_{2,3}$ excitation bands are with medium intensities; but the $5d_{4,5}$ levels are evidently higher than the CBM, therefore the $4f$-$5d_{4,5}$ excitation bands are very weak due to auto-ionization processes.[3]

Herein, the centroid energy of Ce^{3+} ions 5d states in $LiSr_4(BO_3)_3$ is estimated to be ~4.87 eV by calculating the arithmetic average energy of five $4f$-$5d$ excitation bands, which is larger than that in borate $LiCaBO_3$ (4.46 eV, C_1 point symmetry $[CaO_7]$ polyhedron with mean bond length 2.428 Å), close to $LaBO_3$ (4.92 eV, C_s point symmetry $[LaO_9]$ polyhedron with average bond distance 2.602 Å), but smaller than $NaSr_4(BO_3)_3$ (5.15 eV, C_2 point symmetry $[SrO_8]$ polyhedron with mean bond length 2.687 Å) and $Li_6Y(BO_3)_3$ (5.01 eV, C_1 point symmetry $[YO_8]$ polyhedron with average bond distance 2.376 Å).[8,23,25,26] The centroid energy relates to the nephelauxetic effect, the covalency between O^{2-} anions and Ce^{3+} cations and/or the spectroscopic polarizability of O^{2-} anions in the first coordination sphere of Ce^{3+} cations. Above comparisons indicate that Ce^{3+} ions possess a moderate spectroscopic polarizability, covalency and nephelauxetic effect in host compound $LiSr_4(BO_3)_3$.

In terms of the energy difference between the first 5d ($5d_1$) and the fifth 5d ($5d_5$) states in Ce^{3+} ions, the crystal field splitting energy (E_{cfs}) is calculated to be ~2.27 eV (18.3×10^3 cm^{-1}), which is affected by the shape and size of the first anion coordination polyhedron around Ce^{3+} cations. Generally, the smaller coordination number and the shorter bond length will lead to a larger E_{cfs}. For the Ce^{3+} occupying six-coordinated sites in some host compounds, the E_{cfs} values are in the range of $18.6 \times 10^3 - 23.3 \times 10^3$ cm^{-1} and with the arithmetic average value of 20.1×10^3 cm^{-1}. Whereas, for Ce^{3+} ions at eight-fold sites in some host compounds the E_{cfs} have been reported in the range from 16.2×10^3 cm^{-1} to 19.6×10^3 cm^{-1} and with the mean value of about 17.8×10^3 cm^{-1}.[8,27] The later average value is closer to that in our case (18.1×10^3 cm^{-1}), which implies that the spectral data we obtained above may relate to the Ce^{3+} ions in eight-fold coordinated C_2 symmetry Sr^{2+} sites in $LiSr_4(BO_3)_3$.

The above viewpoint can be further verified by the theoretical simulations of 4f-5d$_j$ (j = 1-5) transitions of Ce^{3+} ions. Figure 3 (c, d) shows the calculated 4f-5d$_j$ (j = 1-5) transition energies of Ce^{3+} ions in Sr^{2+} sites when the coordination number (C.N.) of Sr^{2+} is eight and that is six in $LiSr_4(BO_3)_3$, respectively. The calculated and experimental results are also listed in Table 2 for comparison. It is obvious that the experimental excitation spectrum can be attributed to the 4f-5d transitions of Ce^{3+} ions in eight-coordinated Sr^{2+} sites, indicating that the Ce^{3+} ions preferentially occupy eight-coordinated rather than six-coordinated Sr^{2+} sites.

Table 2. The calculated and experimental 4f-5d$_j$ (j = 1-5) transition energies of Ce^{3+} ions

5d multiplets	Calculated (eV)		Experimental (eV)
	six-coordination	eight-coordination	
$5d_1$	3.57	3.84	3.74

14

5d$_2$	3.57	4.42	4.33
5d$_3$	3.87	4.62	4.64
5d$_4$	6.03	5.52	5.61
5d$_5$	6.03	5.96	6.01

The calculation of the relative formation energy can give explanation for the preferential occupancy of Ce^{3+} in two Sr^{2+} sites. The formation energy of Ce^{3+} ions at $[Sr(1)O_6]$ sites is higher than that at $[Sr(2)O_8]$ sites by 0.51 eV, from which it is estimated that the concentration of the latter is higher than the former by more than 2 orders of magnitudes, in agreement with the assignment determined from the excitation spectrum in Figure 3.

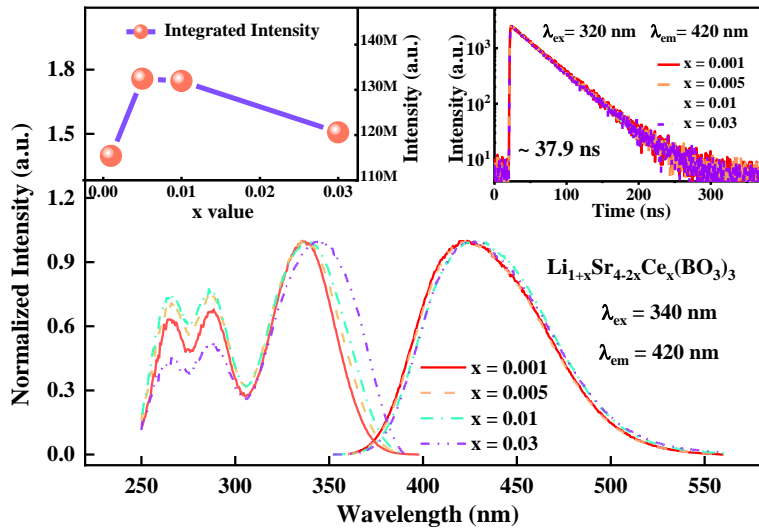### 3.4. Concentration Dependent Luminescence of LiSr$_4$(BO$_3$)$_3$:Ce^{3+}.

Figure 4. The highest height-normalized emission (λ_{ex} = 340 nm) and excitation (λ_{em} = 420 nm) spectra of Li$_{1+x}$Sr$_{4-2x}$Ce$_x$(BO$_3$)$_3$ (x = 0.001, 0.005, 0.01, 0.03) at RT. The insets exhibit the

integrated intensity of emission spectra and the fluorescence decay curves (λ_{ex} = 320 nm, λ_{em} = 420 nm) of $Li_{1+x}Sr_{4-2x}Ce_x(BO_3)_3$, respectively.

The highest height-normalized excitation spectra of $Li_{1+x}Sr_{4-2x}Ce_x(BO_3)_3$ (x = 0.001, 0.005, 0.01, 0.03) samples are exhibited in the left hand of Figure 4. It can be found that the peak positions of the 4f-5d$_j$ (j = 2, 3) excitation bands keep stable for samples with different doping concentrations, but that of the lowest 4f-5d excitation band gradually shifts to long wavelength side. We assume that this phenomenon is mainly related to the slight increase of the 5d crystal field splitting (CFS) of Ce^{3+} ions, as the smaller radius of Ce^{3+} rather than that of Sr^{2+} results in the contraction of the local coordination environment around Ce^{3+} with the increasing doping contents. The right hand of Figure 4 displays the emission spectra of $Li_{1+x}Sr_{4-2x}Ce_x(BO_3)_3$ (x = 0.001, 0.005, 0.01, 0.03) samples under 340 nm excitation. It can be seen that all spectral profiles are almost identical but they slightly move to long wavelength direction with increasing contents of Ce^{3+}, as a consequence of larger CFS of Ce^{3+} 5d state at higher doping level.

The inset in the upper left corner of Figure 4 presents the integrated emission intensity in the range of 350 – 560 nm as a function of doping concentration, showing that the intensity increases first, reaches maximum at x = 0.005 and then decreases with the increase of concentration. Furthermore, the luminescence decay curves of $Li_{1+x}Sr_{4-2x}Ce_x(BO_3)_3$ (x = 0.001, 0.005, 0.01, 0.03) all overlap as presented at the upper right corner of Figure 4 and they can be well fitted by exponential function with lifetime of proximately ~37.9 ns. This value measured at RT is slightly smaller than that (~41.3 ns) collected at a low-temperature 78 K in Figure 2, due to thermal quenching as discussed in detail in Figure 6 (vide infra). Although the intensity- and decay-dependent luminescence are somewhat inconsistent, the decay curves may provide a better

evidence since many experimental factors influence the spectral measurement results.[28] That is, no concentration quenching occurs in the investigated doping contents.
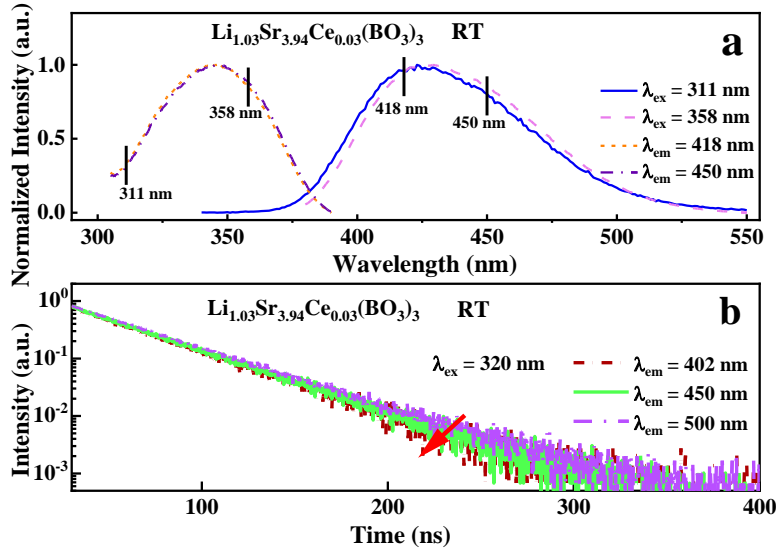

Figure 5. (a) The emission (λ_{ex} = 311, 358 nm) and excitation spectra (λ_{em} = 418, 450 nm) of sample $Li_{1.03}Sr_{3.94}Ce_{0.03}(BO_3)_3$ at RT. (b) the luminescence decay curves (λ_{ex} = 320 nm, λ_{em} = 402, 450, 500 nm) of $Li_{1.03}Sr_{3.94}Ce_{0.03}(BO_3)_3$ at RT.

Figure 2 has illustrated that the inhomogeneous broadening effect is not pronounced in the diluted sample $Li_{1.001}Sr_{3.998}Ce_{0.001}(BO_3)_3$ as mentioned in Section 3.2. It is worthwhile to further assess the inhomogeneous broadening in a concentrated sample to get insight into the influence of doping content on inhomogeneous broadening effect. So, the excitation and emission spectra as well as the luminescence decay curves of the sample $Li_{1.03}Sr_{3.94}Ce_{0.03}(BO_3)_3$, which is with a Ce^{3+} doping concentration 30 times higher than that of $Li_{1.001}Sr_{3.998}Ce_{0.001}(BO_3)_3$, are collected in Figure 5. It can be observed that the highest height-normalized first f-d excitation band ($4f\text{-}5d_1$) is almost invariable when the different emission wavelengths 418 nm and 450 nm are monitored, but the

emission band shifts slightly to long wavelength direction as the excitation wavelength moves from left side 311 nm to right side 358 nm across the first f-d excitation peak (Figure 5a). One of the possible reasons for the observations may be that the inhomogeneous broadening effect is somewhat enhanced in this concentrated sample $Li_{1.03}Sr_{3.94}Ce_{0.03}(BO_3)_3$ in comparison to that in diluted sample $Li_{1.001}Sr_{3.998}Ce_{0.001}(BO_3)_3$.[29,30]

The existence of inhomogeneous broadening in this concentrated sample can be further corroborated by the fluorescence decay curves under 320 nm excitation and different wavelengths emission. When the monitored emission wavelength shifts from 500 to 450 and 402 nm, the decay rate of Ce^{3+} luminescence is faster gradually and the lifetime is shorter steadily as shown in Figure 5b. The shorter the monitored emission wavelength, the faster the luminescence decay, and the shorter the luminescence lifetime. There are some unevenly distributed disturbed Ce^{3+} sites in the highly doping samples, and the 4f-5d transition energies of these ions are slightly different, individually. The successive site-to-site energy transfer provides a channel to change the luminescence lifetime. So the decay time changes with detection wavelength across the emission band and the luminescence decay curve deviates from the exponential form more or less.[31-33]

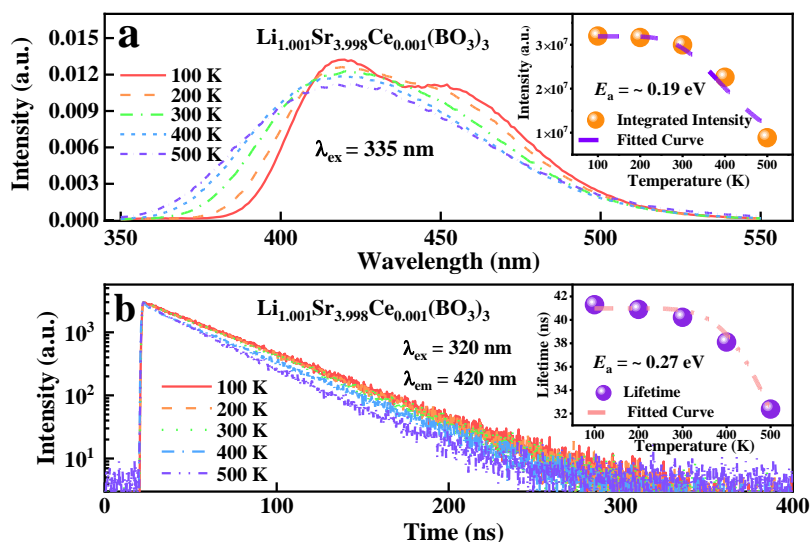**3.5. Luminescence of $Li_{1.001}Sr_{3.998}Ce_{0.001}(BO_3)_3$ at Different Temperatures.**

Figure 6. The normalized emission spectra (a, λ_{ex} = 335 nm) and the luminescence decay curves (b, λ_{ex} = 320 nm, λ_{em} = 420 nm) of $Li_{1.001}Sr_{3.998}Ce_{0.001}(BO_3)_3$ at 100 – 500 K. The insets are the integrated intensity or lifetime as a function of temperature and their fitting results using equations (1, 2), respectively.

Upon 335 nm excitation, the temperature-dependent emission spectra of $Li_{1.001}Sr_{3.998}Ce_{0.001}(BO_3)_3$ sample are measured at the range of 100 – 500 K as shown in Figure 6a. With the increasing temperature, the typical double emission peaks of Ce^{3+} ions gradually merged into a single peak gradually as normal cases. The inset shows that the integrated emission intensity keeps almost stable below 300 K, and then decreases with the increasing temperatures, indicating that the thermal quenching of Ce^{3+} luminescence occurs in $LiSr_4(BO_3)_3$. The thermal quenching can be also confirmed by the temperature-dependent luminescence decay curves of $Li_{1.001}Sr_{3.998}Ce_{0.001}(BO_3)_3$ sample. As shown in Figure 6b, three fluorescence decay curves almost

overlap with each other in the temperature range of 100 – 300 K. Then, the decay begins to get faster above 300 K.

According to the temperature-dependent intensity or lifetime in the insets of Figure 6, the thermal quenching activation energy of Ce^{3+} f-d emission in $LiSr_4(BO_3)_3$ can be evaluated by the single-barrier-quenching model derived equations 1, 2.

$$I(T) = \frac{I_0}{1 + (\frac{\Gamma_0}{\Gamma_v})\exp(^{-E_{(a,I)}}/_{kT})} \tag{1}$$

$$\tau(T) = \frac{\frac{1}{\Gamma_v}}{1 + \frac{\Gamma_0}{\Gamma_v}\exp(^{-E_{(a,\tau)}}/_{kT})} \tag{2}$$

Where I(T) and τ(T) are the integrated emission intensity and lifetime at temperature T K, respectively. Γ_0 and Γ_v are the thermal-quenching rate at $T = \infty$ (attempt rate) and the radiative Ce^{3+} 5d → 4f transition rate, respectively. $E_{(a,I)}$ and $E_{(a,\tau)}$ represents the activation energies for thermal quenching of Ce^{3+} luminescence deduced by intensity and life time, respectively. k is the Boltzmann constant (8.62×10^{-5} eV·K^{-1}). Therefore, the values of $E_{(a,I)}$ and $E_{(a,\tau)}$ are simulated to be ~0.19 eV and ~0.27 eV for this diluted sample $Li_{1.001}Sr_{3.998}Ce_{0.001}(BO_3)_3$, respectively.

The luminescence of 4f-5d transitions of Ce^{3+} and/or Eu^{2+} ions may be thermally-quenched by different nonradiative channels.[28,34-37] Three mechanisms were proposed to explain the thermal-quenching characteristics of Ce^{3+}-doped phosphors.

Initially, the non-radiation 5d → 4f crossover relaxation via electron-phonon coupling is thought to be responsible for the thermal quenching of Ce^{3+} luminescence. In terms of this viewpoint, the

activation energy of thermal quenching corresponds to the energy barrier (E_{fd}) between the lowest point of the excited state 5d parabola and the intersection point of 4f and 5d parabolas in the configurational coordinate diagram. Accordingly, the energy barrier (E_{fd}) in present case is estimated according to the equation 3.[35]

$$E_{fd} = \frac{E_{em}^2}{4E_{FC}} \tag{3}$$

Where the E_{em} is the emission energy 2.99 eV (415 nm) in our case and the E_{FC} is the Franck - Condon shift (0.38 eV), which is approximately equal to half of the Stokes shift (~0.75 eV).[38] So, the value of E_{fd} is 5.88 eV in sample $Li_{1.001}Sr_{3.998}Ce_{0.001}(BO_3)_3$. Apparently, the crossing energy barrier is so large that the 5d → 4f crossover mechanism is unlikely to cause the thermal quenching of Ce^{3+} emission in $LiSr_4(BO_3)_3$ host compound.

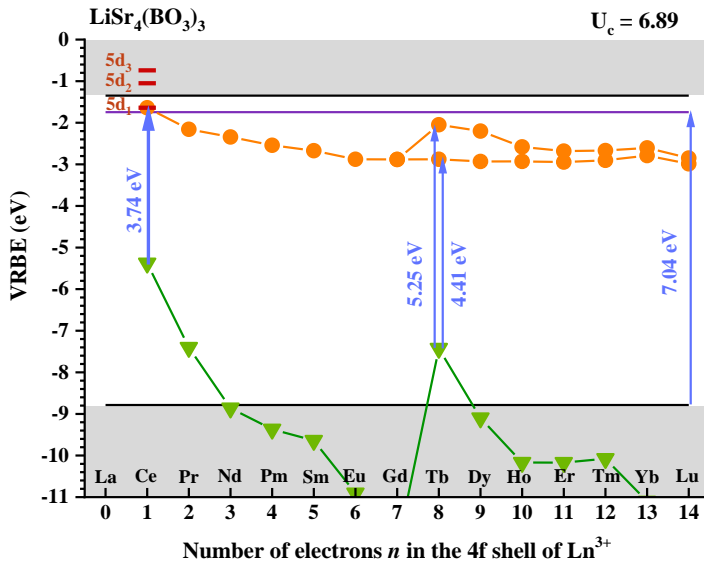**Figure 7.** The vacuum referred binding energy (VRBE) scheme of trivalent lanthanide ions in $LiSr_4(BO_3)_3$. The upper and lower black solid lines are the conduction band minimum (CBM) and

the valence band maximum (VBM), respectively. The distance between the purple line and upper black solid line corresponds to the electron-hole binding energy. The green triangles and orange circles represent the lowest 5d states and 4f ground states of Ln^{3+}, respectively.

Latterly, the thermal ionization of the 5d electrons of Ce^{3+} ions into the conduction band of the host compound has been considered to be the channel resulting in the thermal-quenching of Ce^{3+}. In this scenario, the activation energy of thermal quenching should be close to the energy barrier (E_{dc}) between the lowest 5d of Ce^{3+} and the conduction band minimum of the host compound. To derive this energy barrier (E_{dc}) in $LiSr_4(BO_3)_3$ host compound, the vacuum referred binding energy (VRBE) scheme is constructed as depicted in Figure 7.[3] The adopted experimental data for the construction include the bandgap energy (~7.44 eV) of $LiSr_4(BO_3)_3$ compound, the energies (3.74 eV, 4.33 eV, 4.64 eV, 5.61 eV, 6.01 eV) of Ce^{3+} 4f-5d transitions and the exchange splitting energy (0.84 eV) of Tb^{3+} electron transitions between the low spin and high spin in $LiSr_4(BO_3)_3$ host as displayed in Figure S2. Additional empirical datum involves a Coulomb interaction U_c value of 6.89 eV, which corresponds to the energy difference between the 4f ground states of Eu^{2+} and Eu^{3+} ions and calculated from the chemical shift model.[3] The VRBE scheme reveals the E_{dc} value of Ce^{3+} is 0.29 eV, which is near the experimental fitting values (~0.19 and 0.27 eV, with mean value 0.23±0.04 eV) from the temperature-dependent intensity or lifetime in the insets of Figure 7. Several such factors as the relaxation of 4f-5d transition, the construction of VRBE scheme, the fitting of the thermal quenching activation energy and so on would impose influences on this difference. Anyway, the values are enough to explain the thermal quenching mechanism we focused here. Hence, we assume that electron thermal-ionization process provides an important channel for Ce^{3+} thermal quenching in $Li_{1.001}Sr_{3.998}Ce_{0.001}(BO_3)_3$. In addition, the thermally activated concentration quenching may also contribute to the thermal quenching. In this process,

nonradiative energy migration happen among doping luminescence centers and finally to killer centers like oxygen vacancies or holes in materials[28,35,37] with the increasing temperatures, closely relating to the resonance energy transfer process.[39] With the increase of doping concentration, the spectral overlap between excitation band and emission band usually increases. Consequently, the energy transfer probability between doping ions and that to the quenching centers increase, which eventually results in the decrease of the thermal quenching temperature and the thermal quenching activation energy.

To assess the influence of this factor to the thermal quenching, the temperature-dependent emission spectra and luminescence decay curves of a concentrated sample $Li_{1.03}Sr_{3.94}Ce_{0.03}(BO_3)_3$ are measured at 100 – 500 K as shown in Figure S3. The fitted values of $E_{(a,I)}$ and $E_{(a,\tau)}$ are ~0.15 eV and ~0.18 eV, respectively. The values are slightly smaller than the corresponding values of the diluted $Li_{1.001}Sr_{3.998}Ce_{0.001}(BO_3)_3$ sample. It seems that the thermally activated concentration quenching partially contribute to the thermal quenching of luminescence of Ce^{3+} in $LiSr_4(BO_3)_3$.

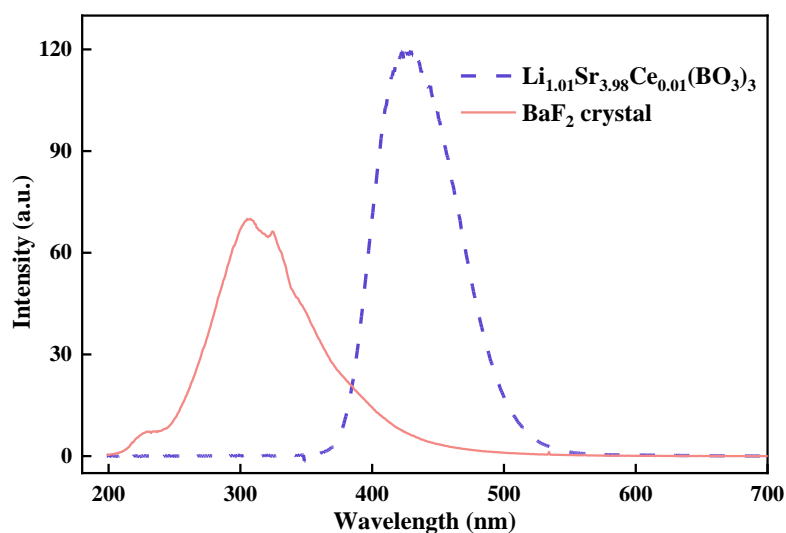**3.6. X-ray Excited Luminescence of $Li_{1.01}Sr_{3.98}Ce_{0.01}(BO_3)_3$.**

Figure 8. The X-ray excited luminescence (XEL) spectra of BaF_2 crystal and $Li_{1.01}Sr_{3.98}Ce_{0.01}(BO_3)_3$ sample at RT.

The X-ray excitation luminescence (XEL) measurement of $Li_{1.01}Sr_{3.98}Ce_{0.01}(BO_3)_3$ sample is performed to evaluate the potential detecting application. The XEL spectra of $Li_{1.01}Sr_{3.98}Ce_{0.01}(BO_3)_3$ compound and BaF_2 reference single crystal at RT are shown in Figure 8. The emission spectrum of $Li_{1.01}Sr_{3.98}Ce_{0.01}(BO_3)_3$ sample exhibits a broad band at the range of 350 – 550 nm, which is consistent with that under UV light excitation. The emission curve of BaF_2 reference single crystal is in agreement with that in reference 14. By calculating the ratio of the integrated intensity of two samples, the photon yield of $Li_{1.01}Sr_{3.98}Ce_{0.01}(BO_3)_3$ sample is estimated to be around 12.0×10^3 photon/MeV using the photon yield 8800 photon/MeV of the BaF_2 reference crystal. This value is also higher than that of commercial $Bi_4Ge_3O_{12}$ powder (8200 photon/MeV).[40] The $Li_{1.01}Sr_{3.98}Ce_{0.01}(BO_3)_3$ powder is worth further optimization as a potential X-ray detecting material.

4. CONCLUSIONS

In this paper, the site occupancy, VUV-UV-vis photoluminescence and X-ray radio-luminescence of Ce^{3+} ions doped in $LiSr_4(BO_3)_3$ are systematically studied, after the sample preparation by a traditional high-temperature solid-state reaction approach and the phase purity and structure characterization by the high-resolution XRD Rietveld refinement. Firstly, the bandgap energy of the host compound is estimated to be ~7.44 eV according to the synchrotron radiation VUV-UV excitation spectra of Ce^{3+} and Gd^{3+}-doped $LiSr_4(BO_3)_3$. Besides, the excitation bands of Ce^{3+} ions in $LiSr_4(BO_3)_3$ are observed around at 331, 286, 267, 221 and 206 nm, and attributed to the transitions to the five 5d crystal field states of Ce^{3+} ions located at the eight-fold coordinated Sr^{2+} sites with C_2 symmetry, not those six-fold coordinated sites. Secondly, the preferential occupancy of Ce^{3+} ions is further confirmed by the calculated 4f-5d$_j$ (j = 1-5) transition energies of Ce^{3+} ions located at both of two sites in the first-principles framework, as there is a good agreement of the experimental results with the calculated ones for the eight-fold coordinated case (31.0×10^3 cm^{-1}, 35.7×10^3 cm^{-1}, 37.3×10^3 cm^{-1}, 44.5×10^3 cm^{-1} and 48.1×10^3 cm^{-1}), and a large mismatch with the six-fold coordinated case (28.8×10^3 cm^{-1}, 28.8×10^3 cm^{-1}, 31.2×10^3 cm^{-1}, 48.6×10^3 cm^{-1} and 48.6×10^3 cm^{-1}). Moreover, the preferential occupancy can be explained by the calculated relative defect formation energies (0.51 and 0.00 eV) of Ce^{3+} located at $[Sr(1)O_6]$ and $[Sr(2)O_8]$ sites, respectively. Thirdly, the doping concentration- and the temperature- dependent luminescence are investigated by the luminescence spectra and decay curves, respectively. There is no concentration quenching for the studied doping concentration range, but the inhomogeneous broadening effect is observed. By the systematic analysis of the thermal quenching activation energies fitted from the experimental spectroscopic data using three kinds of thermal quenching mechanism models, the thermal-ionization mechanism from the 5d states to the host's conduction

band bottom is thought to be predominately responsible for the thermal quenching effect observed, although the potential contribution of the thermal activated concentration quenching is not completely ignored. Finally, the photon yield around 12.0×10^3 photon/MeV of $Li_{1.01}Sr_{3.98}Ce_{0.01}(BO_3)_3$ sample estimated from XEL measurement demonstrates its potential applications in X-ray detecting.

ASSOCIATED CONTENT

Supporting Information

The VUV-UV excitation and emission spectra of $Li_{1.001}Sr_{3.998}Gd_{0.001}(BO_3)_3$, the VUV excitation spectrum of $Li_{1.001}Sr_{3.998}Tb_{0.001}(BO_3)_3$ at 11 K, the normalized emission spectra and luminescence decay curves of a concentrated sample $Li_{1.03}Sr_{3.94}Ce_{0.03}(BO_3)_3$ at 100 – 500 K, the fitting results of integrated intensity and lifetime as a function of temperature, respectively.

This information is available free of charge at the website http://pubs.acs.org

AUTHOR INFORMATION

Corresponding Author

Hongbin Liang − *MOE Key Laboratory of Bioinorganic and Synthetic Chemistry, KLGHEI of Environment and Energy Chemistry, School of Chemistry, Sun Yat-sen University, Guangzhou 510006, China;* orcid.org/0000-0002-3972-2049; Email: cesbin@mail.sysu.edu.cn

Authors

Yunlin Yang − *MOE Key Laboratory of Bioinorganic and Synthetic Chemistry, KLGHEI of Environment and Energy Chemistry, School of Chemistry, Sun Yat-sen University, Guangzhou 510006, China*

Bibo Lou − *CAS Key Laboratory of Microscale Magnetic Resonance and School of Physical Sciences, University of Science and Technology of China, Hefei 230026, China*

Yiyi Ou − *MOE Key Laboratory of Bioinorganic and Synthetic Chemistry, KLGHEI of Environment and Energy Chemistry, School of Chemistry, Sun Yat-sen University, Guangzhou 510006, China;* orcid.org/0000-0002-2111-5064

Fang Su − *MOE Key Laboratory of Bioinorganic and Synthetic Chemistry, KLGHEI of Environment and Energy Chemistry, School of Chemistry, Sun Yat-sen University, Guangzhou 510006, China*

Chong-Geng Ma − *School of Optoelectronic Engineering & CQUPT-BUL Innovation Institute, Chongqing University of Posts and Telecommunications, Chongqing 400065, China;* orcid.org/0000-0001-8090-1738

Chang-Kui Duan − *CAS Key Laboratory of Microscale Magnetic Resonance and School of Physical Sciences, University of Science and Technology of China, Hefei 230026, China;* orcid.org/0000-0003-1016-4976

Pieter Dorenbos − *Faculty of Applied Sciences, Delft University of Technology, 2629 JB, Delft, The Netherlands;* orcid.org/0000-0002-1004-8353

Notes

The authors declare no competing financial interest.

ACKNOWLEDGMENT

REFERENCES

(1) Yen, W. M.; Shionoya, S.; Yamamoto, H. *Phosphor Handbook, Second Edition*; CRC Press, Boca Raton, 2006.

(2) Qin, X.; Liu, X.; Huang, W.; Bettinelli, M.; Liu, X. Lanthanide-Activated Phosphors Based on 4f-5d Optical Transitions: Theoretical and Experimental Aspects. *Chem. Rev.* **2017**, *1175*, 4488–4527.

(3) Dorenbos, P. Improved parameters for the lanthanide $4f^q$ and $4f^{q-1}5d$ curves in HRBE and VRBE schemes that takes the nephelauxetic effect into account. *J. Lumin.* **2020**, *222*, No. 117164.

(4) Dorenbos, P. Fundamental Limitations in the Performance of Ce^{3+}-, Pr^{3+}-, and Eu^{2+}- Activated Scintillators. *IEEE Trans. Nucl. Sci.* **2010**, *57*, 1162–1167.

(5) Xie, M.; Wei, H.; Wu, W. Site Occupancy Studies and Luminescence Properties of Emission Tunable Phosphors $Ca_9La(PO_4)_7$:Re (Re = Ce^{3+}, Eu^{2+}). *Inorg. Chem.* **2019**, *58*, 1877–1885.

(6) Tong, X.; Han, J.; Cai, R.; Xu, Y.; Wu, P.; Zhou, H.; Zhang, X. Multisite-Occupancy-Driven Efficient Multiple Energy Transfer: A Straightforward Strategy to Achieve Single-Composition White-Light Emission in Ce^{3+}-, Tb^{3+}-, and Mn^{2+}-Doped Silicate Phosphors. *Inorg. Chem.* **2020**, *59*, 9838–9846.

(7) Fan, P.; Xu, Z.; Luo, Q.; He, Z.; Chen, Y.; Miao, Q.; Huang, C.; Liu, X.; Li, L. Theoretical Calculation of Bond Energy, Self-Reduction Phenomenon, and Photoluminescence Properties of Eu/Ce Single-Doped and Codoped $Ba_2CaB_2Si_4O_{14}$ Phosphors. *J. Phys. Chem. C* **2021**, *125*, 17820–17830.

(8) Dorenbos, P. 5d-level energies of Ce^{3+} and the crystalline environment. III. Oxides containing ionic complexes. *Phys. Rev. B* **2001**, *64*, 125117–125118.

(9) Zhou, W.; Pan, F.; Zhou, L.; Hou, D.; Huang, Y.; Tao, Y.; Liang, H. Site Occupancies, Luminescence, and Thermometric Properties of $LiY_9(SiO_4)_6O_2:Ce^{3+}$ Phosphors. *Inorg. Chem.* **2016**, *55*, 10415–10424.

(10) Wen, J.; Wang, Y.; Jiang, G.; Zhong, J.; Chu, J.; Xia, Q.; Zhang, Q.; Ning, L.; Duan, C.-K.; Yin, M. First-Principles Study on Self-Activated Luminescence and $4f \rightarrow 5d$ Transitions of Ce^{3+} in $M_5(PO_4)_3X$ (M = Sr, Ba; X = Cl, Br). *Inorg. Chem.* **2020**, *59*, 5170–5181.

(11) Jing, W.; Liu, M.; Wen, J.; Ning, L.; Yin, M.; Duan, C.-K. First-principles study of Ti-doped sapphire. II. Formation and reduction of complex defects. *Phys. Rev. B* **2021**, *104*, No. 165104.

(12) Wu, L.; Chen, X. L.; Li, H.; He, M.; Xu, Y. P.; Li, X. Z. Structure Determination and Relative Properties of Novel Cubic Borates MM'$_4$(BO$_3$)$_3$ (M = Li, M' = Sr; M = Na, M' = Sr, Ba). *Inorg. Chem.* **2005**, *44*, 6409–6414.

(13) Coelho, A. A. *TOPAS Academic*, Ver. 4; Coelho Software: Brisbane, Australia, 2005.

(14) Zhou, R.; Ma, F.; Su, F.; Ou, Y.; Qi, Z.; Zhang, J.; Huang, Y.; Dorenbos, P.; Liang, H. Site occupancies, VUV-UV-vis photoluminescence and X-ray radioluminescence of Eu^{2+} doped $RbBaPO_4$. *Inorg. Chem.* **2020**, *59*, 17421–17429.

(15) Perdew, J. P.; Burke, K.; Ernzerhof, M. Generalized gradient approximation made simple. *Phys. Rev. Lett.* **1996**, *77*, 3865–3868.

(16) Cai, J.; Jing, W.; Cheng, J.; Zhang, Y.; Chen, Y.; Yin, M.; Yeung, Y.-Y.; Duan, C.-K. First-principles calculations of photoluminescence and defect states of Ce^{3+}-doped $(Ca/Sr)_2B_5O_9Cl$. *Phys. Rev. B* **2019**, *99*, No. 125107.

(17) Momma, K.; Izumi, F. VESTA 3 for three-dimensional visualization of crystal, volumetric and morphology data. *J. Appl. Crystallogr.* **2011**, *44*, 1272–1276.

(18) Shannon, R. D. Revised Effective Ionic Radii and Systematic Studies of Interatomic Distances in Halides and Chalcogenides. *Acta Cryst.* **1976**, *A32*, 751–767.

(19) Setlur, A.A.; Srivastava, A.M. On the relationship between emission color and Ce^{3+} concentration in garnet phosphors. *Opt. Mater.* **2007**, *29*, 1647–1652.

(20) Zhang, X.; Lang, H.; Seo, H. J. On the luminescence of Ce^{3+}, Eu^{3+}, and Tb^{3+} in Novel Borate $LiSr_4(BO_3)_3$. *J. Fluoresc.* **2011**, *21*, 1111–1115.

(21) Guo, C.; Ding, X.; Seo, H. J.; Ren, Z.; Bai, J. Luminescent properties of UV excitable blue emitting phosphors $MSr_4(BO_3)_3:Ce^{3+}$ (M = Li and Na). *J. Alloys Compd.* **2011**, *509*, 4871–4874.

(22) Wang, Q.; Deng, D.; Hua, Y.; Huang, L.; Wang, H.; Zhao, S.; Jia, G.; Li, C.; Xu, S. Potential tunable white-emitting phosphor $LiSr_4(BO_3)_3:Ce^{3+}$, Eu^{2+} for ultraviolet light-emitting diodes. *J. Lumin.* **2012**, *132*, 434–438.

(23) Ding, X.; Liang, H.; Hou, D.; Jia, S.; Su, Q.; Sun, S.; Tao, Y. Site occupancy and luminescence of Ce^{3+} in $NaSr_4(BO_3)_3$. *J. Phys. D: Appl. Phys.* **2012**, *45*, No. 365301.

(24) Dorenbos P. Charge transfer bands in optical materials and related defect level location. *Opt. Mater.* **2017**, *69*, 8–22.

(25) Zhou, W.; Hou, D.; Pan, F.; Zhang, B.; Dorenbos, P.; Huang, Y.; Tao, Y.; Liang, H. VUV-vis photoluminescence, X-ray radioluminescence and energy transfer dynamics of Ce^{3+} and Pr^{3+} doped $LiCaBO_3$. *J. Mater. Chem. C* **2015**, *3*, 9161–9169.

(26) Ou, Y.; Zhou, W.; Hou, D.; Brik, M. G.; Dorenbos, P.; Huang, Y.; Liang, H. Impacts of 5d electron binding energy and electron-phonon coupling on luminescence of Ce^{3+} in $Li_6Y(BO_3)_3$. *RSC Adv.* **2019**, *9*, 7908–7915.

(27) Aloui-Lebbou, O.; Goutaudier, C.; Kubota, S.; Dujardin, C.; Cohen-Adad, M.T.; Pédrini, C.; Florian, P.; Massiot, D. Structural and scintillation properties of new Ce^{3+}-doped alumino-borate. *Opt. Mater.* **2001**, *16*, 77–86.

(28) Bachmann, V.; Ronda, C.; Meijerink, A. Temperature Quenching of Yellow Ce^{3+} Luminescence in YAG:Ce. *Chem. Mater.* **2009**, *21*, 2077–2084.

(29) Kodama, N.; Yamaga, M.; Henderson, B. Inhomogeneous broadening of the Ce^{3+} luminescence in $CaYAlO_4$. *J. Phys. Condens. Matter* **1996**, *8*, 3505–3512.

(30) Yamaga, M; Imai, T; Miyairi, H; Kodama, N. Substitutional disorder and optical spectroscopy of Ce^{3+}-doped $CaNaYF_6$ crystals. *J. Phys. Condens. Matter* **2001**, *13*, 753–764.

(31) Lee, S.; Sohn, K.-S. Effect of inhomogeneous broadening on time-resolved photoluminescence in $CaAlSiN_3$: Eu^{2+}. *Opt. Lett.* **2010**, *35*, 1004–1006.

(32) Duan, C.-K.; Tanner, P. A.; Makhov, V.; Khaidukov, N. Emission and Excitation Spectra of Ce^{3+} and Pr^{3+} Ions in Hexafluoroelpasolite Lattices. *J. Phys. Chem. A* **2011**, *115*, 8870–8876.

(33) Leaño, J. L.; Lesniewski, T.; Lazarowska, A.; Mahlik, S.; Grinberg, M.; Sheu, H.-S.; Liu, R.-S. Thermal Stabilization and Energy Transfer in Narrow-band Red-emitting $Sr[(Mg_2Al_2)_{1-y}(Li_2Si_2)_yN_4]$:$Eu^{2+}$ Phosphors. *J. Mater. Chem. C* **2018**, *6*, 5975–5983.

(34) Dorenbos P. Thermal quenching of Eu^{2+} 5d-4f luminescence in inorganic compounds. *J. Phys. Condens. Matter* **2005**, *17*, 8103–8111.

(35) Jia, Y.; Miglio, A.; Poncé, S.; Mikami, M.; Gonze, X. First-principles study of the luminescence of Eu^{2+}-doped phosphors. *Phys. Rev. B* **2017**, *96*, No. 125132.

(36) Lin, Y.-C.; Marco B.; Maths K. Unraveling the mechanisms of thermal quenching of luminescence in Ce^{3+}-doped garnet phosphors. *Chem. Mater.* **2019**, *31*, 3851–3862.

(37) Linderälv, C.; Daniel Å.; Paul E. Luminescence quenching via deep defect states: A recombination pathway via oxygen vacancies in Ce-doped YAG. *Chem. Mater.* **2020**, *33*, 73–80.

(38) Alkauskas, A.; Matthew D. M.; Van de Walle, C. G. Tutorial: Defects in semiconductors—Combining experiment and theory. *J. Appl. Phys.* **2016**, *119*, No. 181101.

(39) Di Bartolo, B. *Advances in Nonradiative Processes in Solids*; Springer, New York, 1991.

(40) Weber, M. J. Inorganic scintillators: today and tomorrow. *J. Lumin.* **2020**, *100*, 35–45.

For Table of Contents Only
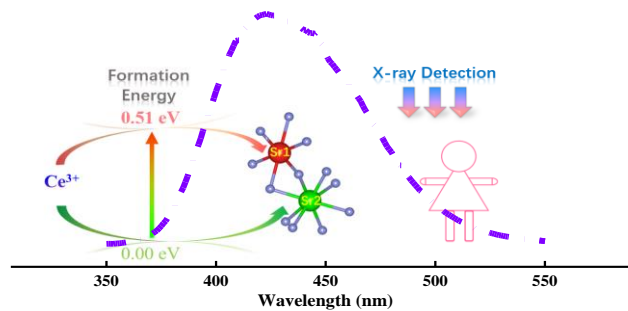
The work provides a systematic method to get insight into the site occupancies of doping ions in the host compounds by the combination of VUV-UV-vis spectral experiments at cryogenic temperatures and theoretical calculations in the first-principles framework using Ce^{3+} doped $LiSr_4(BO_3)_3$ as an example, and demonstrates the potential application of this phosphor in X-ray detection.